



CHORUS

This is the accepted manuscript made available via CHORUS. The article has been published as:

Optical Gating of Resonance Fluorescence from a Single Germanium Vacancy Color Center in Diamond

Disheng Chen, Zhao Mu, Yu Zhou, Johannes E. Fröch, Abdullah Rasmit, Carole Diederichs, Nikolay Zheludev, Igor Aharonovich, and Wei-bo Gao

Phys. Rev. Lett. **123**, 033602 — Published 19 July 2019

DOI: [10.1103/PhysRevLett.123.033602](https://doi.org/10.1103/PhysRevLett.123.033602)

Optical gating of resonance fluorescence from a single germanium vacancy color center in diamond

Disheng Chen,^{1,2,*} Zhao Mu,^{1,*} Yu Zhou,¹ Johannes Froech,³ Abdullah Rasmit,¹ Carole Diederichs,^{4,5} Nikolay Zheludev,^{1,2,6} Igor Aharonovich,^{3,†} and Wei-bo Gao^{1,2,‡}

¹*Division of Physics and Applied Physics, School of Physical and Mathematical Sciences, Nanyang Technological University, Singapore 637371, Singapore*

²*The Photonics Institute and Centre for Disruptive Photonic Technologies, Nanyang Technological University, Singapore 637371, Singapore*

³*School of Mathematical and Physical Sciences, University of Technology Sydney, Ultimo, NSW, 2007, Australia*

⁴*Laboratoire de Physique de l'École normale supérieure, ENS, Université PSL, CNRS, Sorbonne Université, Université Paris-Diderot, Sorbonne Paris Cité, Paris, France*

⁵*MajuLab, International Joint Research Unit UMI 3654, CNRS, Université Côte d'Azur, Sorbonne Université, National University of Singapore, Nanyang Technological University, Singapore*

⁶*Optoelectronics Research Centre, University of Southampton, UK*

(Dated: June 21, 2019)

Scalable quantum photonic networks require coherent excitation of quantum emitters. However, many solid-state systems can undergo a transition to a dark shelving state that inhibits the resonance fluorescence. Here we demonstrate that by a controlled gating using a weak non-resonant laser, the resonant fluorescence can be recovered and amplified for single germanium vacancies (GeV). Employing the gated resonance excitation, we achieve optically stable resonance fluorescence of GeV centers. Our results are pivotal for the deployment of diamond color centers as reliable building blocks for scalable solid state quantum networks.

Artificial atomic systems that can be coherently controlled and manipulated are of a paramount importance for realization of scalable quantum photonic architectures [1, 2]. Recently, color centers in diamond, particularly group IV defects, such as the silicon vacancies (SiV) [3] or the germanium vacancies (GeV) [4–9] have emerged as attractive candidates. These defects possess an inversion symmetry [10] and therefore are not sensitive to local fluctuation in electric fields, resulting in a robust optical fluorescence with high indistinguishability [11]. Additional advantage of those systems is their high Debye-Waller factor that is manifested in a significant portion of the emission being concentrated in the zero phonon line (ZPL) [5, 12]. This high concentration makes their resonance fluorescence (RF) appealing for efficient long-distance quantum communication [13], quantum teleportation [14] and entanglement swapping [15].

Unfortunately, under resonant excitation, these systems can undergo a non-radiative transition to a dark state, resulting in a quenching of RF. For the nitrogen vacancy (NV) centers [16], this is often associated with a charge-state transition from negative to neutral [17, 18]. Such a process results in lack of photons under resonant excitation, and consequently hinder the potential for single-shot spin readout [19, 20], and continuous operation of the quantum network [21]. Here we show that the quenching of RF also occurs for GeV color centers. In the positive side, we find that the RF can be reinstated by employing a small amount of non-resonant beam at 532 nm without inducing any additional spectral diffusion on the quantum emitter. This laser acts as a gate control over the fluorescence from the emitter, which can

be quantitatively modeled by using a 2-level system accompanied by a dark-state.

The investigated sample consists of implantation-generated GeV centers within an electronic-grade Type IIa diamond [22]. The implanted Ge atom takes the interstitial space between the two empty carbon sites, forming a unique split-vacancy configuration with D_{3d} symmetry, as shown in Fig. 1(a). Due to the strong spin-orbit coupling [23], the ground state (2E_g) and excited state (2E_u) split into a pair of energy levels with two-fold spin-degeneracy at zero magnetic field, leading to the characteristic four-line fine structure in the ZPL emission spectrum at 602 nm [Fig. 1(b)]. To enhance the photon collection efficiency, a half-sphere solid immersion lens (SIL) with a diameter of 5 μm is fabricated on top of the sample by using focused ion (Ga+) beam (FIB) milling before Ge implantation [22, 24], as shown in Fig. 1(c). The sample is mounted on a XYZ piezo-stepper motorized stage housed in a closed-cycle helium-flow cryostat at 5 K. The second-order auto-correlation measurement confirms the singleness of the emitter, as shown in Fig. 1(d).

All optical measurements are performed by using a home-built confocal microscope, as shown in Fig. 1(a). An achromatic microscopic objective with NA=0.9 is placed one focal length away from the sample to focus the excitation beam into the SIL and collect the PL from the emitter. A tunable continuous-wave (cw) laser with a linewidth of < 1 MHz is used to resonantly address the GeV center, and perform photoluminescence excitation (PLE) measurements. A diode-pumped solid-state laser at 532 nm is used for non-resonant excitation of the emitter and gating of RF, enabled by pass-

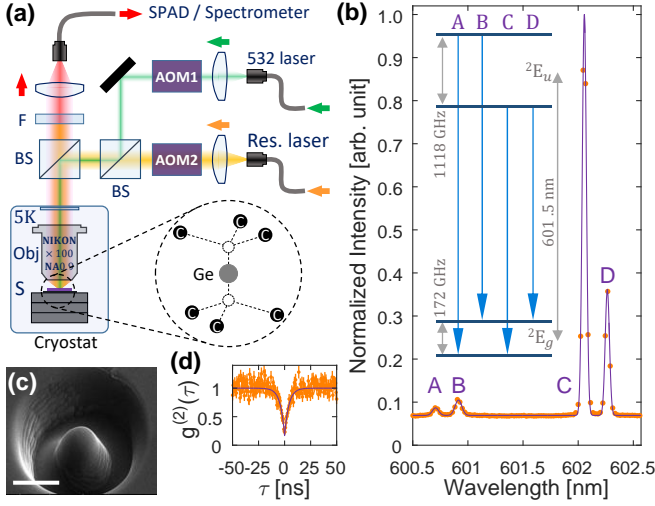


FIG. 1. (a) Experimental setup. AOM: acousto-optic modulator; BS: 50:50 non-polarizing beam splitter; Obj: objective; S: sample; F: spectral filter; SPAD: single-photon avalanche detector. Inset: schematic of a GeV center. (b) Normalized PL spectrum of the GeV color center at 5 K, excited at 532 nm with a power of 0.4 mW ($0.06 P_1$) for an exposure time of 5 s. Purple line is the fitting with four Gaussian peaks, labeled as A, B, C, and D from high to low energy. Inset: energy structure of the GeV center with four optical transitions labeled according to the spectrum. Splitting reflects the best-fit parameters. (c) Scanning electron microscope (SEM) image of a FIB milled SIL. Scale-bar: 3 μm . (d) Room temperature second-order auto-correlation function $g^{(2)}(\tau)$ of the GeV center under non-resonant excitation (532 nm, ~ 1 mW). Fitting with single exponential decay (solid line) gives $g^{(2)}(0) = 0.17 \pm 0.03$.

ing through an acousto-optic modulator (AOM). After directed through a band-pass filter, the PL is coupled into a single-mode fiber connected to a spectrometer or a single-photon avalanche detector (SPAD). In PL spectrum characterization, a 600 ± 7 nm band-pass filter is used for ZPL detection; in PLE and gating experiments, a 650 ± 20 nm band-pass filter is used for phonon-side band (PSB) PL detection.

The gating effect by the non-resonant laser can be demonstrated by comparing PLE spectra with the gating laser on or off, as shown in Fig. 2(a). For both transitions C and D, the PLE spectra are only detectable when the gating laser is on. The PL intensity is enhanced by 500 folds when switching on the gating laser, as shown in Fig. 2(b), where the gating power is $\sim 10^{-4}$ of non-resonant saturation power $P_1 = 6.8 \pm 0.1$ mW [22]. In fact, this non-resonant beam is too weak to induce any detectable fluorescence from the emitter [right panel of Fig. 2(b)], and the main role played by this light is a switch controlling the on and off of the RF from the emitter. By normalizing the PL intensity to the number of photons in the gating beam, we find that 405 nm non-resonant beam generates a nearly-identical gating ef-

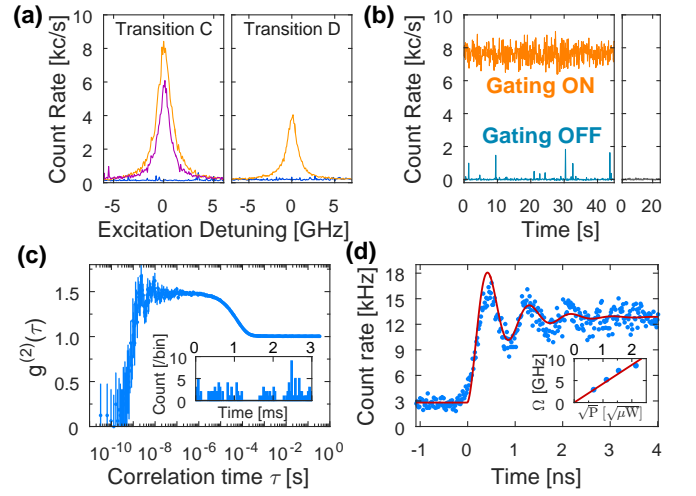


FIG. 2. (a) PLE spectra of transitions C (left) and D (right) when the gating laser at 532 nm is on (orange) and off (blue). Purple curve corresponds to the gating wavelength at 405 nm. Zero detuning corresponds to 602.2903 nm and 602.4828 nm for C and D, respectively. (b) RF intensity of transition C for gating on (orange) and gating off (blue). Right: PL intensity under solely non-resonant excitation. Background has been subtracted from the data. Binsize: 100 ms. (c) $g^{(2)}(\tau)$ of the GeV center under resonant pumping of transition C. $g^{(2)}(0) = 0.07$. The oscillatory signal at $\tau \approx 5$ ns is the Rabi oscillations induced by resonant pumping. Inset: Stochastic jump of the RF. Binsize: 33 μs . (d) Rabi oscillations of transition C in pulsed measurement. Red curve is a fitting by the 2-level system [22]. Inset: Rabi frequency against the square root of resonant power with a linear fit (red). Resonant power is 200 nW for (a)~(b), 300 nW for (c), and 2.4 μW for (d). Non-resonant power is 1.2 μW ($1.8 \times 10^{-4} P_1$) for all.

iciency as of 532 nm [22], as shown in Fig. 2(a).

We stress that the optical pumping between the two ground states cannot account for these observations because the orbital relaxation, $T_1^{\text{orbital}} \simeq 20$ ns [25], is orders of magnitude faster than the gating dynamics involved here. Instead, a long-lived dark state is resorted for the explanation, evident by the bunching plateau of second-order correlation function and the stochastic jumping of RF, as shown in Fig. 2(c) [26, 27]. Even with the presence of a dark state, coherence between the ground and excited states can still be generated and maintained for a coherence time of $T_2 = 366 \pm 20$ ps, as shown by the Rabi oscillations of transition C in Fig. 2(d). Since we do observe multiple peaks around transition C for some measurements (see Fig. S5(a) in Supplementary Material [22]), we focus on transition D for the rest of the Letter for the sake of clarity. The extra peaks in Fig. S5(a) possibly originate from the nearby GeV centers, whose associated D lines are shifted out of the measurement window thanks to the different impacts by the strain on transitions C and D [22, 28, 29].

To understand the photodynamics in the system, we

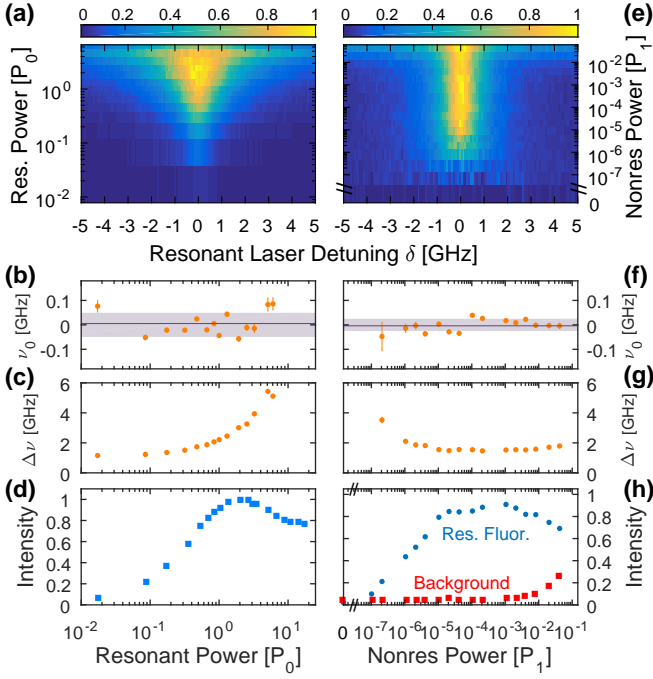


FIG. 3. 2D map of normalized PLE spectra (transition D) by varying (a) the resonant excitation power, or (e) the non-resonant excitation power. Normalization constant: (a) 10 kcnt/s, and (e) 4 kcnt/s. Gating power in (a): $7 \times 10^{-5} P_1$; resonant power in (e): $0.35 P_0$. (b) and (f) are the center frequency ν_0 of each line in (a) and (e), respectively, extracted from Lorentzian fitting. The shaded region represents the standard deviation of ν_0 , (b) $\sigma \sim 50$ MHz, and (f) $\sigma \sim 25$ MHz. (c) and (g) are the Lorentzian linewidth $\Delta\nu$ of each line in (a) and (e), respectively. (d) Resonant-power dependence of RF, measured by setting the resonant laser at zero detuning. (h) Gating-power dependence of RF (blue), evaluated by subtracting the background from the maximum count rate of each line in (e). Background count rate (red) is measured at a far-detuning of ~ 10 GHz.

study the power dependence of RF by varying either the resonant [Fig. 3(a)] or gating power [Fig. 3(e)]. By fitting each line with a Lorentzian function, we obtain a constant transition energy for different resonant powers [Fig. 3(b)], and observe a pronounced power-broadening [Fig. 3(c)]. Meanwhile, the RF intensity displays an unconventional power dependence characterized by an unexpected drop at $\sim 3 P_0$, as shown in Fig. 3(d), where $P_0 = 1.15 \pm 0.39 \mu\text{W}$ is the resonant saturation power, determined by employing a pulse measurement scheme [22]. The drop of RF verifies the existence of a dark state, and indicates the opposite role played by the resonant laser to the gating beam, i.e., shelving the population into the dark state.

As the gating power increases, the initially irresolvable PLE spectrum starts to recover and then stabilizes at $\sim 10^{-5} P_1$ [Fig. 3(e)]. Through the evolution, the transition shows an exceptional stability by displaying zero drift of transition energy [Fig. 3(f)], and an unvarying excitation linewidth [Fig. 3(g)]. This superior optical

property stems from the inversion symmetry of GeV center [25], and shows a striking contrast to the significant spectral diffusion displayed by NV centers under non-resonant excitation [30]. We attribute the broadening of linewidth for low gating powers ($< 10^{-6} P_1$) to the detuning dependence of shelving efficiency of entire system. Since the shelving becomes significantly stronger for smaller detuning (given a constant de-shelving rate), it causes a flattening of PLE spectrum, and gives rise to a wider linewidth [22]. This is similar to the linewidth broadening observed in SiV center at milli-kelvin temperature, where spin pumping plays the role of shelving [31]. As the gating power increases, the gating-based dynamical rates are enhanced and finally dominate the population dynamics, thus stabilizing the linewidth to a constant value. When the gating power exceeds $10^{-3} P_1$, the RF intensity starts to drop, which is accompanied by a rising of PLE background produced by non-resonant excitation [Fig.3(h)]. This reveals a competition between the resonant and non-resonant excitations.

The shelving effect induced by the resonant laser can be directly observed by modulating the resonant beam while keeping the non-resonant beam in cw-mode, as shown in Fig. 4(a). The immediate exponential decay of RF following the excitation edge directly monitors the shelving process. The intensity of the transient peak reflects the population in the excited state before it is influenced by the shelving process induced by the resonant pumping. The subsequent plateau corresponds to the equilibrium state of the system dictated by both shelving and de-shelving rates. Following this phenomenological picture, we construct a 3-state model composed of a 2-level system (G and E) and a dark state (D), as shown in Fig. 4(b). The population in the ground state (G) can be resonantly promoted (Ω) to the excited state (E), before relaxing back to the ground state via spontaneous decay (Γ_{sp}), or being shelved into a dark state (D) via a non-radiative channel (k_{ED}). The ground and dark state can exchange the population at rates k_{DG} and k_{GD} , mainly enabled by non-resonant pumping. Within the framework of semi-classical picture, the time-evolution of the system follows the master equation

$$\frac{d}{dt} \begin{pmatrix} \rho_{\text{G}} \\ \rho_{\text{E}} \\ \rho_{\text{GE}} \\ \rho_{\text{EG}} \\ \rho_{\text{D}} \end{pmatrix}^{\text{T}} = \begin{pmatrix} -k_{\text{GD}} & \Gamma_{\text{sp}} & i\Omega/2 & -i\Omega/2 & k_{\text{DG}} \\ 0 & -\Gamma_{\text{sp}} - k_{\text{ED}} & -i\Omega/2 & i\Omega/2 & 0 \\ i\Omega/2 & -i\Omega/2 & -1/T_2 & 0 & 0 \\ -i\Omega/2 & i\Omega/2 & 0 & -1/T_2 & 0 \\ k_{\text{GD}} & k_{\text{ED}} & 0 & 0 & -k_{\text{DG}} \end{pmatrix} \begin{pmatrix} \rho_{\text{G}} \\ \rho_{\text{E}} \\ \rho_{\text{GE}} \\ \rho_{\text{EG}} \\ \rho_{\text{D}} \end{pmatrix} \quad (1)$$

where ρ_{G} , ρ_{E} , and ρ_{D} are the time-dependent population in ground, excited and dark state, ρ_{GE} and ρ_{EG} are the coherence between G and E, Ω is the resonant Rabi frequency, Γ_{sp} is the spontaneous decay rate, and T_2 is

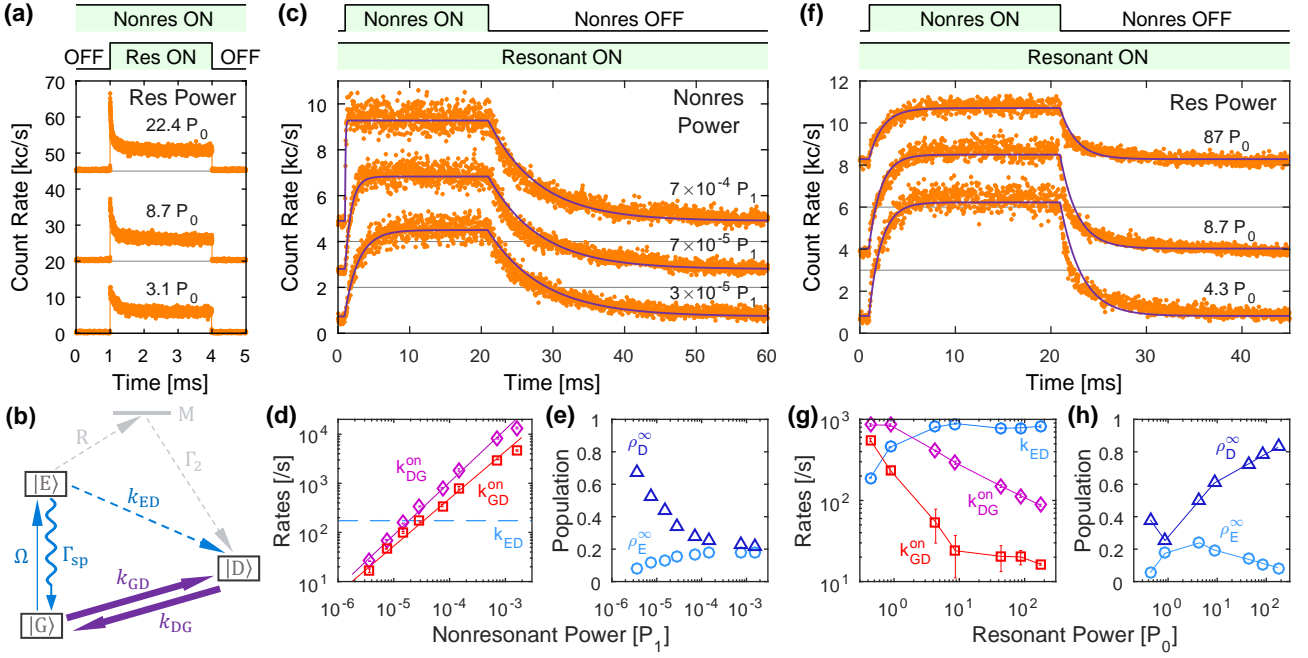


FIG. 4. Gating and shelving dynamics. (a) Time-resolved PL by modulating the resonant beam with constant non-resonant power of $7 \times 10^{-7} P_1$. (b) Physical model. G, E, D and M: ground, excited, dark, and metastable state; k_{GD} , k_{DG} and k_{ED} : population transfer rates from G to D, D to G, and E to D. Ω : resonant Rabi frequency; $\Gamma_{sp} = 1/T_1 = 280$ MHz: spontaneous decay rate, determined by lifetime measurement [22]. Grey arrows depict the possible physical processes underlying k_{ED} . (c) and (f) are the time-resolved PL by modulating the non-resonant beam with (c) constant resonant power ($0.9 P_0$) or (f) constant non-resonant power ($7 \times 10^{-5} P_1$). Black curves are the fittings by using Eqn. 3. (d) and (g) are the dynamical rates extracted from the fittings in (c) and (f), respectively. Dashed blue horizontal lines in (d) depicts k_{ED} , representing its trivial non-resonant power dependence in this experiment. Solid straight lines in (d) are the fittings with $k_{GD}^{on} = 3.5 \times 10^6 \times P^{0.96}$ (red) and $k_{DG}^{on} = 2.1 \times 10^7 \times P^{1.07}$ (purple), where P denotes the non-resonant power in the unit of P_1 . (e) and (h) are the on-period steady-state population of dark state ρ_D^∞ and 2-level system ρ_E^∞ , evaluated by using the rates in (d) and (g), respectively. In (a), (c) and (f), raw data (orange dots) are vertically shifted for clarity, with the zero-intensity level indicated by the grey horizontal lines. Top panel: modulation protocol.

the coherence time of excited state. Note that Eqn. 1 has incorporated the effect of stimulated emission, which is expected to play a non-trivial role in population dynamics of the system. The excitation linewidth can be derived from the steady-state solution of Eqn. 1

$$\Delta\nu = \frac{1}{\pi T_2} \sqrt{1 + \frac{1}{2} \frac{\Omega^2 T_2}{\Gamma_{sp} + k_{ED}} \left(1 + \frac{k_{ED} + k_{DG}}{k_{DG} + k_{GD}}\right)} \quad (2)$$

in the unit of linear frequency. By equalizing the asymptotic linewidth at $0 P_0$ in Fig. 3(c) (~ 1 GHz, 20 times of lifetime-limited value) to Eqn. 2 with $\Omega = 0$, we obtain $T_2 = 316 \pm 20$ ps, which is consistent with the coherence time extracted from the Rabi oscillations measurement [Fig. 2(d)]. The detected RF intensity follows

$$I_{PL}(t) = \eta \Gamma_{sp} \rho_E(t) \quad (3)$$

where $\eta = 9 \times 10^{-5}$ is the overall efficiency including both detection efficiency of the experimental setup and quantum yield of GeV center [22, 32].

To extract the dynamical rates of gating and shelving, we perform a similar time-resolved experiment, but

modulating the non-resonant beam while keeping the resonant beam in cw mode. Here, the PL inherits the modulation pattern of the gating laser, and displays a gating-power-dependent modulation depth, as shown in Fig. 4(c). Since the non-resonant laser has little effect on k_{ED} , we keep this rate a constant and determine it via global fitting [22]. The main effect of the gating beam is to promote k_{GD} and k_{DG} linearly over the non-resonant power, as shown in Fig. 4(d). This power dependence implies a single-photon process for the shelving and deshelling of population induced by the non-resonant laser. Consequentially, the steady-state population is transferred from the dark state to the ground and excited states as increasing the gating power, as shown in Fig. 4(e).

Resonant power dependence is shown in Fig. 4(f). The main effect of the resonant laser is to speed up the shelving rate k_{ED} , while indirectly reducing rates k_{GD} and k_{DG} , as shown in Fig. 4(g). The saturation behavior of k_{ED} implies a two-step shelving process mediated by a meta-stable state M, as shown by the grey arrows in Fig. 4(b). The first step of population pumping (R) from

the excited state to the meta-stable state is responsible for the enhancement of k_{ED} , while the second step of non-radiative decay (Γ_2) from the metastable state to the dark state caps k_{ED} at kHz regime. The peak of steady-state population ρ_E^∞ at several P_0 in Fig. 4(h) suggests the optimal resonant power for the maximum RF given a gating power.

Now we briefly discuss the photophysics of the GeV system by comparing it to NV centers in diamond [17, 33] and InGaAs self-assembled quantum dots (QD) [34, 35], where a similar phenomenon has been observed. For both systems, the dark state has been identified as a differently charged species of the emitter, specifically, positively charged QD [26] and neutrally charged NV center [36]. It is hence plausible that the dark state of the GeV center is also a differently charged state (i.e., neutral) [23]. For all three systems, the gating of RF can be achieved by employing a small amount of non-resonant beam. The mechanism for NV centers and QDs involves a local free-charge-carrier bath produced by the light, which can modify the charge dynamics of the emitter in favor of resonant excitation. We argue a similar mechanism for GeV center as long as non-resonant laser is employed, which is substantiated by two observations: linear power dependence of k_{DG} and k_{GD} [Fig. 4(d)], and identical gating efficiency for 405 nm and 532 nm non-resonant beams [Fig. 2(a)].

On the other hand, the shelving mechanism induced by resonant pumping is different. For QDs, no such a shelving channel is reported. For NV centers, a two-photon process is involved based on the quadratic power dependence of the dynamical rates [17, 18]. For GeV center, a two-step shelving mechanism pivot by a metastable state and non-radiative decay channel is identified in this Letter. Finally, the decrease of rates k_{GD} and k_{DG} in Fig. 4(g) is possibly related to the decrease of free charge carrier density, caused by the presence of more charge traps in the area as induced by a stronger resonant beam [22].

In summary, we demonstrated the shelving effect induced by the resonant laser in GeV centers, which can be counteracted by introducing a weak non-resonant repumping laser. The dynamics of shelving and gating can be quantitatively explained by the presence of a dark state, while the identity of this dark state warrants future investigation. We stress that this gating phenomenon is quite general and ubiquitous, not limited to the specific center investigated in this Letter [22]. The recovery and stabilization of the RF could be useful for quantum information science and scalable quantum photonics, such as spin-photon entanglement [37, 38] and photon-photon interferences [11].

We acknowledge Singapore NRF fellowship grant (NRF-NRFF2015-03) and NRF QEP grant, Singapore Ministry of Education (MOE2016-T2-2-077, MOE2016-T2-1-163 and MOE2016-T3-1-006 (S)), A*Star QTE

programme, the Australian Research Council (via DP180100077), the Asian Office of Aerospace Research and Development grant FA2386-17-1-4064, the Office of Naval Research Global(N62909-18-1-2025) and the AFAiIR node of the NCRIS Heavy Ion Capability for access to ion-implantation/ion-beam analysis facilities.

* These two authors contributed equally

† igor.aharonovich@uts.edu.au

‡ wbgao@ntu.edu.sg

- [1] I. Aharonovich and E. Neu, *Advanced Optical Materials* **2**, 911 (2014).
- [2] M. Atatre, D. Englund, N. Vamivakas, S.-Y. Lee, and J. Wrachtrup, *Nature Reviews Materials* **3**, 38 (2018).
- [3] E. Neu, D. Steinmetz, J. Riedrich-Müller, S. Gsell, M. Fischer, Matthias Schreck, and C. Becher, *New Journal of Physics* **13**, 025012 (2011).
- [4] T. Iwasaki, F. Ishibashi, Y. Miyamoto, Y. Doi, S. Kobayashi, T. Miyazaki, K. Tahara, K. D. Jahnke, L. J. Rogers, B. Naydenov, F. Jelezko, S. Yamasaki, S. Nagamachi, T. Inubushi, N. Mizuochi, and M. Hatano, *Scientific Reports* **5**, 12882 (2015).
- [5] Y. N. Palyanov, I. N. Kupriyanov, Y. M. Borzdov, and N. V. Surovtsev, *Scientific Reports* **5**, 14789 (2015).
- [6] S. Huler, G. Thiering, A. Dietrich, N. Waasem, T. Teraji, J. Isoya, Takayuki Iwasaki, M. Hatano, F. Jelezko, A. Gali, and A. Kubanek, *New Journal of Physics* **19**, 063036 (2017).
- [7] M. Bhaskar, D. Sukachev, A. Sipahigil, R. Evans, M. Burek, C. Nguyen, L. Rogers, P. Siyushev, M. Metsch, H. Park, F. Jelezko, M. Lonar, and M. Lukin, *Physical Review Letters* **118**, 223603 (2017).
- [8] H. Siampour, S. Kumar, V. A. Davydov, L. F. Kulikova, V. N. Agafonov, and S. I. Bozhevolnyi, *Light: Science & Applications* **7**, 61 (2018).
- [9] K. Bray, B. Regan, A. Trycz, R. Previdi, G. Seniutinas, K. Ganesan, M. Kianinia, S. Kim, and I. Aharonovich, *ACS Photonics* **5**, 4817 (2018).
- [10] C. Hepp, T. Müller, V. Waselowski, J. N. Becker, B. Pingault, H. Sternschulte, D. Steinmüller-Nethl, A. Gali, J. R. Maze, M. Atatre, and C. Becher, *Physical Review Letters* **112**, 036405 (2014).
- [11] A. Sipahigil, K. Jahnke, L. Rogers, T. Teraji, J. Isoya, A. Zibrov, F. Jelezko, and M. Lukin, *Physical Review Letters* **113**, 113602 (2014).
- [12] E. Neu, M. Fischer, S. Gsell, M. Schreck, and C. Becher, *Physical Review B* **84**, 205211 (2011).
- [13] L.-M. Duan, M. D. Lukin, J. I. Cirac, and P. Zoller, *Nature* **414**, 413 (2001).
- [14] D. Bouwmeester, J.-W. Pan, K. Mattle, M. Eibl, H. Weinfurter, and A. Zeilinger, *Nature* **390**, 575 (1997).
- [15] J.-W. Pan, D. Bouwmeester, H. Weinfurter, and A. Zeilinger, *Physical Review Letters* **80**, 3891 (1998).
- [16] M. W. Doherty, N. B. Manson, P. Delaney, F. Jelezko, J. Wrachtrup, and L. C. L. Hollenberg, *Physics Reports The nitrogen-vacancy colour centre in diamond*, **528**, 1 (2013).
- [17] G. Waldherr, J. Beck, M. Steiner, P. Neumann, A. Gali, T. Frauenheim, F. Jelezko, and J. Wrachtrup, *Physical Review Letters* **106**, 157601 (2011).

- [18] P. Siyushev, H. Pinto, M. Vrs, A. Gali, F. Jelezko, and J. Wrachtrup, *Physical Review Letters* **110**, 167402 (2013).
- [19] D. Sukachev, A. Sipahigil, C. Nguyen, M. Bhaskar, R. Evans, F. Jelezko, and M. Lukin, *Physical Review Letters* **119**, 223602 (2017).
- [20] A. N. Vamivakas, C.-Y. Lu, C. Matthiesen, Y. Zhao, S. Flt, A. Badolato, and M. Atatire, *Nature* **467**, 297 (2010).
- [21] H. J. Kimble, *Nature* **453**, 1023 (2008).
- [22] See Supplementary Material, which includes etxra Refs.[39-42].
- [23] G. Thiering and A. Gali, *Physical Review X* **8**, 021063 (2018).
- [24] L. Marseglia, J. P. Hadden, A. C. Stanley-Clarke, J. P. Harrison, B. Patton, Y.-L. D. Ho, B. Naydenov, F. Jelezko, J. Meijer, P. R. Dolan, J. M. Smith, J. G. Rarity, and J. L. OBrien, *Applied Physics Letters* **98**, 133107 (2011).
- [25] P. Siyushev, M. H. Metsch, A. Ijaz, J. M. Binder, M. K. Bhaskar, D. D. Sukachev, A. Sipahigil, R. E. Evans, C. T. Nguyen, M. D. Lukin, P. R. Hemmer, Y. N. Palyanov, I. N. Kupriyanov, Y. M. Borzdov, L. J. Rogers, and F. Jelezko, *Physical Review B* **96**, 081201 (2017).
- [26] H. S. Nguyen, G. Sallen, M. Abbarchi, R. Ferreira, C. Voisin, P. Roussignol, G. Cassabois, and C. Diederichs, *Physical Review B* **87**, 115305 (2013).
- [27] A. Delteil, W.-b. Gao, P. Fallahi, J. Miguel-Sanchez, and A. Imamolu, *Physical Review Letters* **112**, 116802 (2014).
- [28] S. Maity, L. Shao, Y.-I. Sohn, S. Meesala, B. Machielse, E. Bielejec, M. Markham, and M. Lonar, *Physical Review Applied* **10**, 024050 (2018).
- [29] S. Meesala, Y.-I. Sohn, B. Pingault, L. Shao, H. A. Atikian, J. Holzgrafe, M. Gndoan, C. Stavarakas, A. Sipahigil, C. Chia, R. Evans, M. J. Burek, M. Zhang, L. Wu, J. L. Pacheco, J. Abraham, E. Bielejec, M. D. Lukin, M. Atatire, and M. Lonar, *Physical Review B* **97**, 205444 (2018).
- [30] J. Wolters, N. Sadzak, A. W. Schell, T. Schrder, and O. Benson, *Physical Review Letters* **110**, 027401 (2013).
- [31] J. N. Becker, B. Pingault, D. Gro, M. Gndoan, N. Kukharchyk, M. Markham, A. Edmonds, M. Atatire, P. Bushev, and C. Becher, *Physical Review Letters* **120**, 053603 (2018).
- [32] K. N. Boldyrev, B. N. Mavrin, P. S. Sherin, and M. N. Popova, *Journal of Luminescence* **193**, 119 (2018), special Issue in honor of Professor Renata Reisfeld for her outstanding contributions to luminescent inorganic glasses.
- [33] K.-M. C. Fu, C. Santori, P. E. Barclay, and R. G. Beausoleil, *Applied Physics Letters* **96**, 121907 (2010).
- [34] H. S. Nguyen, G. Sallen, C. Voisin, P. Roussignol, C. Diederichs, and G. Cassabois, *Physical Review Letters* **108**, 057401 (2012).
- [35] D. Chen, G. R. Lander, K. S. Krowpman, G. S. Solomon, and E. B. Flagg, *Physical Review B* **93**, 115307 (2016).
- [36] N. Aslam, G. Waldherr, P. Neumann, F. Jelezko, and J. Wrachtrup, *New Journal of Physics* **15**, 013064 (2013).
- [37] E. Togan, Y. Chu, A. S. Trifonov, L. Jiang, J. Maze, L. Childress, M. V. G. Dutt, A. S. Srensen, P. R. Hemmer, A. S. Zibrov, and M. D. Lukin, *Nature* **466**, 730 (2010).
- [38] K. De Greve, L. Yu, P. L. McMahon, J. S. Pelc, C. M. Natarajan, N. Y. Kim, E. Abe, S. Maier, C. Schneider, M. Kamp, S. Hfling, R. H. Hadfield, A. Forchel, M. M. Fejer, and Y. Yamamoto, *Nature* **491**, 421 (2012).
- [39] [first reference in SM not already in paper] R. Loudon, *The Quantum Theory of Light*, 3rd ed. (Oxford University Press, 2000).
- [40] [third reference in SM not already in paper] Y.-I. Sohn, S. Meesala, B. Pingault, H. A. Atikian, J. Holzgrafe, M. Gndoan, C. Stavarakas, M. J. Stanley, A. Sipahigil, J. Choi, M. Zhang, J. L. Pacheco, J. Abraham, E. Bielejec, M. D. Lukin, M. Atatire, and M. Lonar, *Nature Communications* **9**, 2012 (2018).
- [41] [seventh reference in SM not already in paper] A. V. Turukhin, C.-H. Liu, A. A. Gorokhovskiy, R. R. Alfano, and W. Phillips, *Physical Review B* **54**, 16448 (1996).
- [42] [eighth reference in SM not already in paper] E. Neu, M. Agio, and C. Becher, *Optics Express* **20**, 19956 (2012).